Journal of Physics and Chemistry of Solids 75 (2014) 782–786

Contents lists available at ScienceDirect

Journal of Physics and Chemistry of Solids

journal homepage: www.elsevier.com/locate/jpcs

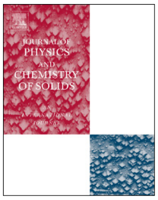

Phase transformation and dielectric characteristics in $Ba_{0.85}Ca_{0.15}Ti_{1-x}(Mg_{1/2}W_{1/2})_xO_3$ ceramics

Jingji Zhang [a], Bei Liu [a], Ludong Ji [a], Jiangying Wang [a,*], Jiwei Zhai [b]

[a] *College of Materials Science and Engineering, China Jiliang University, Hangzhou 310018, China*
[b] *Functional Materials Research Laboratory, Tongji University, Shanghai 200092, China*

ARTICLE INFO

Article history:
Received 30 September 2013
Received in revised form
28 January 2014
Accepted 29 January 2014
Available online 5 February 2014

Keywords:
C. Raman spectroscopy
D. Crystal structure

ABSTRACT

Structure, phase transformation and dielectric properties of $Ba_{0.85}Ca_{0.15}Ti_{1-x}(Mg_{1/2}W_{1/2})_xO_3$ ceramics with $0.02 \le x \le 0.20$ have been investigated by means of X-ray diffraction, Raman and dielectric spectroscopy. X-ray diffraction and Raman results show that $(Mg_{1/2}W_{1/2})^{4+}$ substitution for Ti^{4+} ions results in the formation of a second phase of $BaWO_4$ at $x = 0.05$. Dielectric measurements reveal a gradual transformation from normal ferroelectric characteristics to typical relaxor behaviour. A more reasonable relationship $f = f_0 \exp\left[-(E_a/k_BT_m)^p\right]$ is introduced to characterise the dielectric relaxation, which yields an activation energy with ~27 meV. The high activation energy for the composition with a high $(Mg_{1/2}W_{1/2})^{4+}$ level may be ascribed to more defect pair $[mg''_{Ti} - V''_0]$.

1. Introduction

Barium titanate ($BaTiO_3$), calcium titanate ($CaTiO_3$) and their solid solutions have been extensively studied for potential applications in ferroelectric, piezoelectric and tunable microwave devices due to their excellent electrical properties and being environmentally friendly [1–4] $BaTiO_3$ is the first perovskite-type ferroelectrics, which exhibits three successive structural phase transitions with decreasing temperature: from paraelectric cubic to ferroelectric tetragonal, tetragonal to orthorhombic and orthorhombic to rhombohedra phases at T_{C-T} (~130 °C), T_{T-O} (~0 °C) and T_{O-R} (~−90 °C), respectively.5 $CaTiO_3$, known as incipient ferroelectrics or quantum paraelectrics, can be used to form $Ba_{1-x}Ca_xTiO_3$ solid solutions with x up to 0.21. It causes a negligible change of T_{C-T}, but strongly shifts T_{T-O} to substantially lower temperature, and hence shows great potential for improving its electrical properties [5,6].

Recently, the solid solutions with isovalent-substituted Ti^{4+}, such as $Ba(Ti_{1-x}Zr_x)O_3$ [7] $Ba(Ti_{1-x}Sn_x)O_3$ [8] $(Ba,Ca)(Ti_{1-x}Zr_x)O_3$ [9,10] and $(Ba,Ca)(Ti_{1-x}Sn_x)O_3$ [11] have been studied extensively. These ions can shift T_{T-O} and T_{O-R} of $BaTiO_3$-based ceramics towards higher temperature, and simultaneously lower their T_{C-T} [5] leading to a pinched phase transition [12]. Complex ionic $(B_{1/2}W_{1/2})^{4+}$ (B=Mg and Ni) substitution for Ti^{4+} has been also investigated to improve the electrical properties of $BaTiO_3$ [13–15] This research has focussed on improving the microwave properties by high $(B_{1/2}W_{1/2})^{4+}$ substitution levels. However, little attention has been focussed on their phase transformation behaviour and dielectric properties.

In the present work, therefore, we investigate in a detailed manner the structure, phase transformation and dielectric properties of $Ba_{0.85}Ca_{0.15}Ti_{1-x}(Mg_{1/2}W_{1/2})_xO_3$ ceramics with x up to 0.20 using X-ray diffraction (XRD), Raman and dielectric spectroscopy.

2. Experimental procedure

$Ba_{0.85}Ca_{0.15}Ti_{1-x}(Mg_{1/2}W_{1/2})_xO_3$ ceramics were prepared through the conventional solid-state reactions. Stoichiometric amounts of high-purity $BaCO_3$ (99.0%), $CaCO_3$ (99.0%), TiO_2 (98.0%), MgO (98.0%) and WO_3 (99.9%) powders were mixed and ball-milled with zirconia media in ethanol for 24 h and then dried at 110 °C for 12 h. After drying, the powders were calcined at 1200 °C for 4 h in air and then remilled for 24 h. The calcined powders, mixed with 8 wt% polyvinyl alcohol, were pressed into pellets at 100 MPa. The green pellets were kept at 550 °C for 6 h to remove the solvent as well as the binder and then sintered at 1450 °C for 4 h in air.

Phase compositions of the ceramics were investigated by means of XRD (Bruker D2 Phaser, Germany) with CuK_α radiation. Permittivity (ε) as a function of temperature was measured using an HP 4284 A precision LCR meter (Agilent, Palo Alto, CA, USA) at frequencies from 1 kHz to 1 MHz in the temperature range of 125–450 K. Room-temperature micro-Raman spectra of the

---

[*] Corresponding author. Tel.: +86 571 86875609; fax: +86 571 86875609.
E-mail address: wjyliu@163.com (J. Wang).

http://dx.doi.org/10.1016/j.jpcs.2014.01.023
0022-3697

samples were recorded using a Renishaw inVia spectrometer with the 514.5 nm line of an Ar^{+} laser.

3. Results and discussion

XRD patterns of the $Ba_{0.85}Ca_{0.15}Ti_{1-x}(Mg_{1/2}W_{1/2})_xO_3$ ceramics are given in Fig. 1. The samples with low $(Mg_{1/2}W_{1/2})^{4+}$ substitution levels ($x \leq 0.05$) are single perovskite phase, whereas those with high $(Mg_{1/2}W_{1/2})^{4+}$ levels ($x \geq 0.10$) have additional diffraction lines, which can be assigned to $BaWO_4$ (JCPDS No. 43-0646). The additional $BaWO_4$ phase has been ever detected in the $Ba(Mg_{1/2}W_{1/2})O_3$-$BaTiO_3$ ceramics reported by Takahashi et al. [15] This observation means that high $(Mg_{1/2}W_{1/2})^{4+}$ substitution levels result in the formation of $BaWO_4$ and $Ba_{0.85-x/2}Ca_{0.15}Ti_{1-x}Mg_{x/2}O_3$ phases, that is, for $x=0.20$, $Ba_{0.85}Ca_{0.15}Ti_{0.80}(Mg_{1/2}W_{1/2})_{0.20}O_3 \rightarrow BaWO_4 + Ba_{0.75}Ca_{0.15}Ti_{0.80}Mg_{0.10}O_3$. Simultaneously, based on defect chemistry, defect pair $[mg_{Ti}'' - V_0'']$ is formed in the samples with high (Mg1/2W1/2)4+ substitution levels.

In order to analyse structural evolution of perovskite phase, the (1 1 1), (002, 200) and (202, 220) characteristic peaks are fitted using the Gaussian function by 'XPSPEAK' software (Fig. 2). It can be seen that the composition with $x=0.02$ possesses a tetragonal phase, characterised by the splitting of the (0 0 2)/(2 0 0) peaks at 2θ of ~45°. As the concentration of $(Mg_{1/2}W_{1/2})^{4+}$ increases, the (0 0 2)/(2 0 0) peaks merge into a single peak, whereas no splitting of the (2 2 0) peak at 2θ of ~66° is observed, indicating that the tetragonal-to-cubic phase transformation takes place with increasing $(Mg_{1/2}W_{1/2})^{4+}$ substitution levels.

In addition, the shift of diffraction peaks of the perovskite phase is not obvious with increasing $(Mg_{1/2}W_{1/2})^{4+}$ substitution levels. It is further analysed by showing the variation of unit cell parameters and unit cell volume as a function of x (inset, Fig. 1). As x increases, lattice constant a increases, whereas c reaches a maximum at $x=0.05$ and then decreases. As a whole, unit cell volume increases. When $x \leq 0.05$, a distinct increase in unit cell volume with x is due to the larger $(Mg_{1/2}W_{1/2})^{4+}$ substitution for Ti^{4+}. The ionic radius of Mg^{2+} (0.72 Å) in sixfold coordination is much larger than that of Ti^{4+} (0.605 Å), while that of W^{6+} (0.60 Å) in sixfold coordination is a bit smaller than that of Ti^{4+} (0.605 Å) [16]. Therefore, the ionic radius of the complex cation $(Mg_{1/2}W_{1/2})^{4+}$ (0.66 Å) is larger than that of Ti^{4+}, which leads to the expansion of the crystal cells. When $x \geq 0.10$, the slight increase of unit cell volume can be readily ascribed to the formation of oxygen vacancies [17] and the difference in ion radius between Mg^{2+} and Ti^{4+}. On the one hand, as BaWO$_4$ phase is formed, Ti^{4+} ions are mainly substituted by Mg^{2+} ions, which causes a pronounced lattice expansion. On the other hand, the formation of BaWO4 phase leads to a decrease of Ba/Ca ratio, which is responsible for lattice shrinkage. As shown in Fig. 2, an obvious broadening (≥0.27o) in full width at half maximum (FWHM) of symmetric (1 1 1) peak in the compositions with $x \geq 0.05$ can be observed as compared to that with $x=0.02$ (0.22o), indicating that (Mg1/2W1/2)4+ doping leads to a larger lattice strain, and further destroying the long-range order of the Ba0.85Ca0.15TiO3 lattice [18].

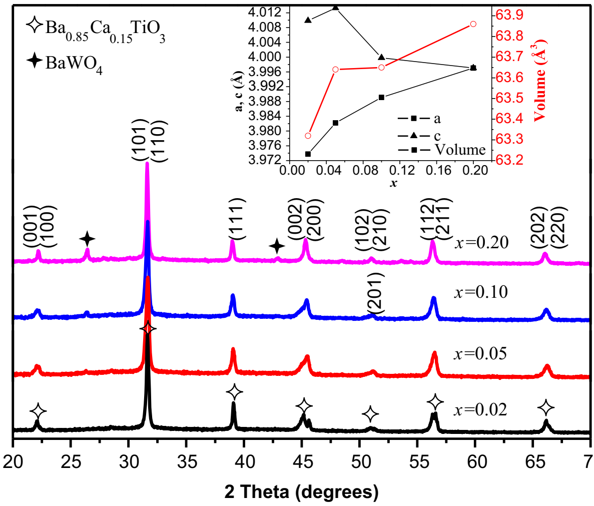

Fig. 1. XRD patterns of the $Ba_{0.85}Ca_{0.15}Ti_{1-x}(Mg_{1/2}W_{1/2})_xO_3$ ceramics. The inset presents the variation of the lattice parameters as a function of x.

Raman spectroscopy is a sensitive and effective technique in characterising material structural variation. Room-temperature Raman spectra of all compositions are illustrated in Fig. 3. Raman spectra of the composition with $x=0.02$ show a sharp and strong band associated with $A_1(TO_3)$ mode at ~520 cm^{-1}, and two asymmetric bands connected with $A_1(TO_2)$ and $A_1(LO_3)/E(LO)$ at ~248 and 726 cm^{-1}, respectively. A strong band at ~125 cm^{-1} should be attributed to a mass effect related to Mg and W ions motion against oxygen octahedra, similar to some doped $BaTiO_3$ system [18–20]. The observed anti-resonance effect at ~176 cm$^{-1,}$ as an interference feature, is attributed to a coupling between two A_1(TO) modes with different types of BO_6 octahedra [18] The band at ~302 cm^{-1}, which is characteristic of a tetragonal phase, is assigned to the B_1+E (TO_2+LO) mode. The peak at ~302 cm^{-1} becomes weak with increasing $(Mg_{1/2}W_{1/2})^{4+}$ substitution levels, suggesting that the tetragonality is decreased with an increase in $(Mg_{1/2}W_{1/2})^{4+}$ substitutions. Meanwhile, the $A_1(TO_2)$ mode broadens and red-shifts, accompanied by the appearance of $A_1(TO_1)$ mode at ~181 cm^{-1}, which results in the disappearance of the interference feature, whereas the $A_1(LO_3)/E(LO)$ mode blue-shifts, indicating that Ba^{2+}/Ca^{2+} ions interact with anions more strongly [21].

The two peaks at ~181 and 302 cm^{-1} become two shoulders of the $A_1(TO_2)$ band in the compositions with $x \geq 0.05$, revealing the existence of local polar ordering and B-site Mg^{2+} defects [18], respectively. Additionally, the sharp bands at ~330, 795 and 925 cm^{-1} in the compositions with $x \geq 0.05$ are associated with $\nu_2(B_g)$, $\nu_3(E_g)$ and $\nu_1(A_g)$ of the $BaWO_4$ phase [22], respectively, which contributes greatly to the decrease in tetragonality. These results are in good agreement with XRD results. Especially, the band at ~833 cm^{-1}, which is also observed in heterovalent-substituted $BaTiO_3$ ceramics [18,20,23], is attributed to a deformation of BO_6 octahedron resulting from the charge difference of different types of ions at equivalent site in $BaTiO_3$.

The temperature dependence of ε for all samples measured at different frequencies, varying from 1 kHz to 1 MHz, is displayed in Fig. 4. The dielectric anomalous peaks of the cubic–tetragonal phase transition (paraelectric–ferroelectric transition) for the $Ba_{0.85}Ca_{0.15}Ti_{1-x}(Mg_{1/2}W_{1/2})_xO_3$ ceramics are markedly suppressed and shifted towards lower temperature with increasing $(Mg_{1/2}W_{1/2})^{4+}$ substitution levels. Meanwhile, the other dielectric peaks of the tetragonal–orthorhombic phase transition are shifted towards higher temperature, leading to a pinched phase transition [12]. This suppression is attributed to the distortion of TiO_6 octahedron. The reduction in the temperature at the permittivity maxima T_m is due to the deterioration of the ferroelectric long-range order.

As shown in Fig. 4, the spectral features closely depend on the composition. The composition with $x=0.02$ shows a sharp and strong dielectric peak at 349 K without frequency dispersion. With increasing $(Mg_{1/2}W_{1/2})^{4+}$ substitution levels, the sharp and strong dielectric peak gradually becomes a diffuse peak with frequency dispersion feature. An obvious shift of T_m towards higher temperature with increasing frequency is observed for $x=0.10$ and 0.20, indicating a typical relaxor behaviour. To compare the width of the phase transition region of all compositions, Fig. 5 shows the reduced permittivity $\varepsilon/\varepsilon_m$ (ε_m is the permittivity maxima) as a